mathematics

MDPI

Article

The Optimal Balance between Oncolytic Viruses and Natural Killer Cells: A Mathematical Approach

Dongwook Kim [1,*], Dong-Hoon Shin [2] and Chang K. Sung [3]

[1] Department of Mathematics, Texas A&M University Kingsville, Kingsville, TX 78363, USA
[2] Department of Global Finance and Banking, Inha University, Incheon 22212, Korea
[3] Department of Biological and Health Sciences, Texas A&M University Kingsville, Kingsville, TX 78363, USA
* Correspondence: dongwook.kim@tamuk.edu

Abstract: Oncolytic virotherapy (OV) is a cancer therapy utilizing lytic viruses that specifically target cancer cells for elimination. In this relatively new therapy, two contradictory observations have been made. Some studies showed that immune responses including activated natural killer (NK) cells post oncolytic viral infection increased the cancer cell death, while others reported that such initial immune responses diminished the anti-tumor efficacy, which was caused by premature viral clearance. In this paper, we present a mathematical model to investigate the effect of NK cells on oncolytic virotherapy. Particularly, we focused on the minimum condition for NK cells to be activated in terms of parameters and how the activation of NK cells interacts and changes the dynamics among cancer, infected cancer cells and oncolytic virus. Analytic works for the existence and stability conditions of equilibrium points are provided. Numerical results are in good agreement with analytic solutions. Our numerical results show that equilibrium points can be created or destroyed by the activation of NK cells in a dynamical system and suggest that the balance between the bursting rate of the virus and the activation rate of NK cells is a crucial factor for successful OV therapy.

Keywords: oncolytic virotherapy; NK cells; bifurcation; dynamical system; mathematical model

MSC: 92B05; 37N25; 34D20



Citation: Kim, D.; Shin, D.-H.; Sung, C.K. The Optimal Balance between Oncolytic Viruses and Natural Killer Cells: A Mathematical Approach. *Mathematics* **2022**, *10*, 3370. https://doi.org/10.3390/math10183370

Received: 19 August 2022
Accepted: 13 September 2022
Published: 16 September 2022

Publisher's Note: MDPI stays neutral with regard to jurisdictional claims in published maps and institutional affiliations.



Copyright: © 2022 by the authors. Licensee MDPI, Basel, Switzerland. This article is an open access article distributed under the terms and conditions of the Creative Commons Attribution (CC BY) license (https://creativecommons.org/licenses/by/4.0/).

1. Introduction

Oncolytic virotherapy employs lytic viruses that specifically target cancer cells for cell lysis while normal cells remain intact. In this relatively new cancer therapy, lytic viruses are usually modified or engineered to limit their replication to cancer cells, thus selectively targeting tumor cells for viral replication and host cell lysis [1–4]. This selectivity toward tumor cells enables developing superior therapeutic approaches to other traditional therapies including radiation and chemotherapy, which are often accompanied by side effects due to unwanted normal cell death [5]. Many genetically modified oncolytic viruses including adenovirus, herpesvirus and measles virus are being tested under various stages of clinical trials [4,6]. Talimogene laherparepvec (T-VEC; IMLYGIC®, Amgen Inc. Thousand Oaks, CA, USA) is the first FDA-approved therapy that utilizes an engineered oncolytic herpes simplex virus, targeting cancer cells for lysis in melanoma patients [7]. In addition, a clinical study with four glioblastoma multiforme (GBM) patients demonstrated the potential of virotherapy for the treatment of GBM [8]. Another GBM clinical study (Phase 1) has been conducted by Desjardins et al. [9]. In this therapeutic approach to reduce glioblastoma recurrence and mortality rates, recombinant polio-rhinovirus particles were employed, and their viral immunotherapy led to higher survival rates compared to controls. A Phase 2 study of this recombinant oncolytic polio-rhinovirus in adult GBM patients is currently underway (NCT02986178).

The infected tumor cells can be eliminated either by direct cell lysis or activated immune responses such as natural killer (NK) cells or T lymphocytes [10–12]. Leung et al.

demonstrated that activated NK cells can increase the efficacy of oncolytic adenoviruses by targeting adeno virus-infected ovarian cancer cells [13]. The hamster model study with oncolytic adenoviruses showed that the tumor cell lysis during viral infection is mainly caused by activated T cell immune responses [14]. Virus-induced immune responses, however, may also kill the virus-infected tumor cells prematurely, before viruses have a chance to make new progeny, diminishing the effects of virotherapy on the elimination of tumor cell population [15,16]. It has been reported that NK cells reduce the efficacy of oncolytic herpes viruses in murine glioblastoma cells [17]. Their further studies also demonstrated that the inhibition of NK cells by TGFβ treatment led to increased viral replication and efficacy as well as reduced tumor growth in the xenograft model of glioblastoma [18]. Altomonte et al. showed that inhibition of the NK-activating ligand CD155 increased the viral efficacy in infected hepatocellular carcinoma cells [19]. The results of these studies indicate that finding the optimal balance between virus-activated immune response and viral reproduction rates is important for successful virotherapy outcomes.

Several mathematical models have been developed to address the interactions among uninfected cancer cells (UC), infected cancer cells (IC), oncolytic viruses (OV) and immune cells and the effect of immune cells on oncolytic virotherapy using a system of differential equations [11,20–26]. For example, Phan and Tian showed the effect of innate immune response on populations of infected cancer cells and free virus [23]. In their model, the bursting size of a virus plays an important role in the population dynamics with innate immune response; more or less, equilibrium points are created depending on a bursting size. Kim et al. investigated the anti-tumoral and anti-viral roles of NK cells in oncolytic virus–bortezomib therapy [20]. Their experimental data and mathematical modeling support that the anti-tumor efficacy increases when either the number of endogenous NK cells decreases or the number of exogenous NK cells increases in the tumor. Al-Tuwairqi et al. proposed the mathematical model for OV with the innate immune system. They modified the model proposed in [23] by introducing an interaction between the innate immune system and uninfected tumor cells, which results in creating more equilibrium points in dynamics [11]. Senekal et al. studied how NK cell recruitment to the tumor microenvironment affects OV therapy. Their results show that OV infection plays important roles in decreasing the tumor size and inducing the strong NK cell response to achieve tumor remission [26].

In this paper, we develop a simple mathematical model of dynamical interactions among cancer cells, infected cancer cells, oncolytic viruses, and virus-induced NK cells. Particularly, our study aims to analyze the dynamics of populations with respect to both the oncolytic virus replication ability and the stimulation of OV-induced NK cells in a simpler setting. We sought to optimize the balance between viral replication efficiency and induction of immune responses for successful virotherapies. Our modeling analyses suggest that strongly induced NK cells kill the infected cells prior to viral replication and cell lysis, reducing the viral population and efficacy of oncolytic virotherapy. Although NK cells are known to promote uninfected tumor cell clearance, our results indicate that the initial viral titer and usage of NK inhibitors should be under consideration not to provoke too much immune responses that may lead to the hyper-activation of innate NK cells, resulting in a reduction in OV efficacy.

2. Materials and Methods

2.1. Model

Experimental and mathematical approaches show that a glioma-selective HSV-1 mutant has a high bursting (replication) ability, which is a crucial factor for the success of virotherapy [23,27–29]. The mathematical compartment model is modified from [29] by adding effects of an NK cell (anti-tumoral and anti-viral effects). The model describes the interaction between cancer cells, infected cancer cells and oncolytic viruses in the presence of the innate immune response, particularly NK cells. The main objectives of the proposed model are to study (1) the role of NK cells in the oncolytic virotherapy and (2) mechanisms underlying how NK cells reduce the efficacy of oncolytic virotherapy.

In this model, we assume that (1) the cancer cell grows logistically at the rates, λ, up to their carrying capacity (K), (2) the oncolytic virus is 100% cancer cell specific, (3) one virus particle infects one cancer cell. Once a virus enters a cancer cell, it is incapable of infecting additional cells and ceases to be part of the free virus population, and (4) NK cells are anti-tumor and anti-viral. The model is given by

$$\begin{array}{l} \frac{dx}{dt} = \lambda x(t)\left(1 - \frac{x(t)}{K}\right) - \alpha x(t)v(t) - \beta x(t)z(t), \\ \frac{dy}{dt} = \alpha x(t)v(t) - \gamma y(t)z(t) - \delta_1 y(t), \\ \frac{dv}{dt} = b\delta_1 y(t) - \alpha x(t)v(t) - \delta_2 v(t), \\ \frac{dz}{dt} = \lambda_z y(t)z(t) - \delta_3 z(t). \end{array} \tag{1}$$

where $x(t)$, $y(t)$, $v(t)$ and $z(t)$ represent the population of cancer cell, infected cancer cell, the free virus and NK cell, respectively. λ is the growth rate of the cancer cell population and K is the carrying capacity tumor size. The term $\lambda x(t)\left(1 - \frac{x(t)}{K}\right)$ describes the logistic growth rate of the cancer cell population $x(t)$. The constant value α represents the strength of infectivity of the virus in the infected cancer cells so that the term αxv describes the rate of infected cells by free virus, $v(t)$. β represents the killing rate of the cancer cells by NK cells and γ is the killing rate of infected cancer cells by NK cells. δ_1 represents the death rate of infected cells after oncolysis. b is the bursting size of free virus particles. δ_2 is the clearance rate of the virus. λ_z is the stimulation rate of the NK cells by infected cancer cells and δ_3 is the clearance rate of NK cells. For convenience, we omit the time-dependence (t) in Equation (1).

For non-dimensionalization, we set $\tau = \delta_1 t$, $x = K\widetilde{x}$, $y = K\widetilde{y}$, $v = K\widetilde{v}$, $z = K\widetilde{z}$. Then,

$$\frac{d\tau}{dt} = \delta_1, \quad \frac{dx}{dt} = \delta_1 K\frac{d\widetilde{x}}{d\tau}, \quad \frac{dy}{dt} = \delta_1 K\frac{d\widetilde{y}}{d\tau}, \quad \frac{dv}{dt} = \delta_1 K\frac{d\widetilde{v}}{d\tau}, \quad \frac{dz}{dt} = \delta_1 K\frac{d\widetilde{z}}{d\tau}. \tag{2}$$

Equation (1) becomes

$$\begin{array}{l} \frac{d\widetilde{x}}{d\tau} = \frac{\lambda}{\delta_1}\widetilde{x}(1-\widetilde{x}) - \frac{\alpha K}{\delta_1}\widetilde{x}\widetilde{v} - \frac{\beta K}{\delta_1}\widetilde{x}\widetilde{z}, \\ \frac{d\widetilde{y}}{d\tau} = \frac{\alpha K}{\delta_1}\widetilde{x}\widetilde{v} - \frac{\gamma K}{\delta_1}\widetilde{y}\widetilde{z} - \widetilde{y}, \\ \frac{d\widetilde{v}}{d\tau} = b\widetilde{y} - \frac{\alpha K}{\delta_1}\widetilde{x}\widetilde{v} - \frac{\delta_2}{\delta_1}\widetilde{v}, \\ \frac{d\widetilde{z}}{d\tau} = \frac{\lambda_z K}{\delta_1}\widetilde{y}\widetilde{z} - \frac{\delta_3}{\delta_1}\widetilde{z}. \end{array} \tag{3}$$

We have the following model by setting the parameters: $r_1 = \frac{\lambda}{\delta_1}$, $a = \frac{\alpha K}{\delta_1}$, $k_1 = \frac{\beta K}{\delta_1}$, $k_2 = \frac{\gamma K}{\delta_1}$, $r_2 = \frac{\lambda_z K}{\delta_1}$, $\delta_v = \frac{\delta_2}{\delta_1}$, and $\delta_z = \frac{\delta_3}{\delta_1}$. For convenience, we write $\widetilde{x} = x$, $\widetilde{y} = y$, $\widetilde{v} = v$, $\widetilde{z} = z$ and $\tau = t$.

$$\begin{array}{l} \frac{dx}{dt} = r_1 x(1-x) - axv - k_1 xz, \\ \frac{dy}{dt} = axv - k_2 yz - y, \\ \frac{dv}{dt} = by - axv - \delta_v v, \\ \frac{dz}{dt} = r_2 yz - \delta_z z. \end{array} \tag{4}$$

Theorem 1. *If initial conditions $x(0) \geq 0$, $y(0) \geq 0$, $v(0) \geq 0$, $z(0) \geq 0$ in some region D, then the solutions of the system in Equation (4), $x(t)$, $y(t)$, $v(t)$ and $z(t)$, are non-negative and $x(t)$ is bounded in D for all $t \geq 0$.*

Proof. Let us rewrite the first equation of the system (4) as $\frac{dx}{x} = (r_1(1-x) - av - k_1 z)dt$. By taking integral over $[0, t]$, we obtain $x(t) = x(0)e^{\int_0^t r_1(1-x) - av - k_1 z\ ds}$. Since $x(0) \geq 0$, we have $x(t) \geq 0$ for all $t \geq 0$. Similarly, $y(t) = y(0)e^{\int_0^t axv - k_2 yz - y\ ds}$, $v(t) = v(0)e^{\int_0^t by - axv - \delta_v v\ ds}$ and $z(t) = z(0)e^{\int_0^t r_2 xz - \delta_z z\ ds}$. Since initial conditions $x(0) \geq 0$, $y(0) \geq 0$, $v(0) \geq 0$, $z(0) \geq 0$, we have $y(t) \geq 0$, $v(t) \geq 0$ and $z(t) \geq 0$ for all $t \geq 0$. Next, we prove that $x(t)$ is bounded. □

From the first equation of the system (4),

$$\frac{dx}{dt} = r_1x(t)(1-x(t)) - ax(t)v(t) - k_1x(t)z(t) \leq r_1x(t)(1-x(t)). \tag{5}$$

Consider $\frac{dX}{dt} = r_1X(t)(1-X(t))$ with initial condition $X(0) = X_0$; then, the solution of the differential equation is $X(t) = \frac{X_0}{X_0+(1-X_0)e^{r_1t}}$. Since $\frac{dx}{dt} \leq \frac{dX}{dt}$, $\lim_{t\to\infty} supX(t) = 1$, we have

$$\lim_{t\to\infty} supx(t) \leq \lim_{t\to\infty} supX(t) = 1.$$

Therefore, all the solutions of system (3) are non-negative, and $x(t)$ is bounded in the following region:

$$D = \{(x,y,v,z) \in R^4 \Big| \ 0 \leq x \leq 1,\ y \geq 0,\ v \geq 0,\ z \geq 0\Big\}.$$

D is the positive invariant where every solution with an initial condition in D remains there for all $t \geq 0$.

2.2. Equilibrium Points

The equilibrium points of the system are obtained by setting the right-hand side of Equation (4) to zero. Let $X = (x,\ y,\ v,\ z)^T$ and

$$F(x) = (r_1x(1-x) - axv - k_1xz,\ axv - k_2yz - y,\ by - axv - \delta_v v,\ r_2yz - \delta_z z)^T.$$

Then, the system can be written as the autonomous system $\frac{dX}{dt} = F(X)$. We assume that the solution set (x,y,v,z) of Equation (4) is in D. Simply, the equilibrium points are the solution of $\frac{dX}{dt} = 0$ or $F(X) = 0$, which is given by

$$\begin{aligned} &r_1x(1-x) - axv - k_1xz = 0,\\ &axv - k_2yz - y = 0,\\ &by - axv - \delta_v v = 0,\\ &r_2yz - \delta_z z = 0. \end{aligned} \tag{6}$$

(1) If $x = 0$, then from the second equation in Equation (6), $y(k_2z+1) = 0$, which implies $y = 0$ since $k_2z + 1 = 0 \Rightarrow z = -\frac{1}{k_2}$. It leads to $v = 0$ and z = 0. Therefore, we have an equilibrium point $E_0(0,\ 0,\ 0,\ 0)$.

(2) If $x \neq 0$ and $z = 0$ from the fourth equation in Equation (6), we obtain $y = axv$ from the second equation and $by = (ax + \delta_v)v$ from the third equation in Equation (6), which leads to $abxv = v(ax + \delta_v) \Rightarrow v(abx - ax - \delta_v) = 0$. If $v = 0$, then we obtain $y = 0$ and $x = 1$ from the first equation in Equation (6). Thus, we have an equilibrium point $E_1(1,\ 0,\ 0,\ 0)$.

(3) If $x \neq 0$, $v \neq 0$ and $z = 0$, then, from the second and third equation in Equation (6), $by = abxv = v(ax - \delta_v) \Rightarrow v(abx - ax - \delta_v) = 0$. Since $v \neq 0$, we have $abx - ax - \delta_v = 0 \Rightarrow x = \frac{\delta_v}{a(b-1)}$. From the first and second equation in Equation (6), $r_1x(1-x) = y \Rightarrow y = \frac{r_1\delta_v}{a(b-1)}\left(1 - \frac{\delta_v}{a(b-1)}\right)$. From the second and third equations in Equation (6), $axv = y = by - \delta_v v \Rightarrow (b-1)y = \delta_v v \ \Rightarrow v = \frac{b-1}{\delta_v}y$, which is $v = \frac{r_1}{a}\left(1 - \frac{\delta_v}{a(b-1)}\right)$. Thus, we have an equilibrium point $E_2(x_2,\ y_2,\ v_2,\ 0)$, where $x_2 = \frac{\delta_v}{a(b-1)}$, $y_2 = \frac{r_1\delta_v}{a(b-1)}\left(1 - \frac{\delta_v}{a(b-1)}\right)$ and $v_2 = \frac{r_1}{a}\left(1 - \frac{\delta_v}{a(b-1)}\right)$.

(4) If $x \neq 0$, $v \neq 0$ and $z \neq 0$, from the fourth equation in Equation (6), $z(r_2y - \delta_z) = 0 \Rightarrow y = \frac{\delta_z}{r_2}$. From the second and third equations in Equation (6), we obtain $by - y - k_2yz$

$-\delta_v v = 0 \Rightarrow k_2 yz = by - y - \delta_v v$. It leads to $z = \frac{b-1}{k_2} - \frac{r_2\delta_v}{k_2\delta_z}v$. From the first equation in Equation (6), we obtain $x = 1 - \frac{k_1(b-1)}{r_1 k_2} + \left(\frac{k_1 r_2 \delta_v - a k_2 \delta_z}{r_1 k_2 \delta_z}\right)v$. Let us define

$$\begin{aligned} x &= x_0 + x_1 v, \\ y &= y_0, \\ z &= z_0 + z_1 v. \end{aligned} \tag{7}$$

where $x_0 = 1 - \frac{k_1(b-1)}{r_1 k_2}$, $x_1 = \frac{k_1 r_2 \delta_v - a k_2 \delta_z}{r_1 k_2 \delta_z}$, $y_0 = \frac{\delta_z}{r_2}$, $z_0 = \frac{b-1}{k_2}$ and $z_1 = \frac{r_2 \delta_v}{k_2 \delta_z}$.

By substituting x, y and z into Equation (6), we have the following quadratic equation

$$a x_1 v^2 + (a x_0 - k_2 y_0 z_1)v - k_2 y_0 z_0 - y_0 = 0.$$

Using the quadratic formula, $v = \frac{-(a x_0 - k_2 y_0 z_1) \pm \sqrt{(a x_0 - k_2 y_0 z_1)^2 - 4 a x_1 (-k_2 y_0 z_0 - y_0)}}{2 a x_1}$. Thus, we have two equilibrium points $E_3(x^*, y^*, v_+^*, z^*)$ and $E_4(x^*, y^*, v_-^*, z^*)$, where $x^* = 1 - \frac{k_1(b-1)}{r_1 k_2} + \left(\frac{k_1 r_2 \delta_v - a k_2 \delta_z}{r_1 k_2 \delta_z}\right)v^*$, $y^* = \frac{\delta_z}{r_2}$, $z^* = \frac{b-1}{k_2} - \frac{r_2 \delta_v}{k_2 \delta_z}v^*$,

$v_+^* = \frac{-(a x_0 - k_2 y_0 z_1) + \sqrt{(a x_0 - k_2 y_0 z_1)^2 - 4 a x_1 (-k_2 y_0 z_0 - y_0)}}{2 a x_1}$

and $v_-^* = \frac{-(a x_0 - k_2 y_0 z_1) - \sqrt{(a x_0 - k_2 y_0 z_1)^2 - 4 a x_1 (-k_2 y_0 z_0 - y_0)}}{2 a x_1}$.

Note that $E_4(x^*, y^*, v_-^*, z^*)$ does not exist in the positive invariant domain D, since all parameters are positive values, which lead to $v_-^* < 0$. Therefore, we do not consider $E_4(x^*, y^*, v_-^*, z^*)$ as an equilibrium point.

2.3. Stability of Equilibrium Points

We investigate the local stability of the equilibrium point using the linearization technique by finding the eigenvalues of the Jacobian matrix of the nonlinear system (4) at an equilibrium point. The Jacobian matrix of the system (4) is given by

$$J(x, y, v, z) = \begin{pmatrix} r_1 - 2r_1 x - av - k_1 z & 0 & -ax & -k_1 x \\ av & -k_2 z - 1 & ax & -k_2 y \\ -av & b & -ax - \delta_v & 0 \\ 0 & r_2 z & 0 & r_2 y - \delta_z \end{pmatrix}$$

Theorem 2. *The equilibrium point $E_0(0, 0, 0, 0)$ is always unstable.*

Proof. The Jacobian matrix of the system (4) at $E_0(0, 0, 0, 0)$ is

$$J(E_0) = \begin{pmatrix} r_1 & 0 & 0 & 0 \\ 0 & -1 & 0 & 0 \\ 0 & b & -\delta_v & 0 \\ 0 & 0 & 0 & -\delta_z \end{pmatrix}$$

The eigenvalues are $\lambda_1 = r_1$, $\lambda_2 = -1$, $\lambda_3 = -\delta_v$ and $\lambda_4 = -\delta_z$. Here, all parameters are positive values, so that the equilibrium point $E_0(0, 0, 0, 0)$ is an unstable point, the stable manifold is tangent to the *y*-*v*-*z* subspace, and the unstable manifold is tangent to the *x*-axis. □

Theorem 3. *The equilibrium point $E_1(1, 0, 0, 0)$ is locally asymptotically stable if $a < \frac{\delta_v}{b-1}$ and is unstable if $a > \frac{\delta_v}{b-1}$.*

Proof. The Jacobian matrix of the system (4) at $E_1(1,\ 0,\ 0,\ 0)$ is

$$J(E_1) = \begin{pmatrix} -r_1 & 0 & 0 & 0 \\ 0 & -1 & a & 0 \\ 0 & b & -a-\delta_v & 0 \\ 0 & 0 & 0 & -\delta_z \end{pmatrix}$$

Solving the characteristic equation, $|J(E_1) - \lambda I| = 0$, we have $\lambda_1 = -r_1$, $\lambda_2 = -\delta_z$ and $\lambda_{3,4}$ satisfy the equation $\lambda^2 + a_1\lambda + a_2 = 0$, where $a_1 = a + \delta_v + 1$ and $a_2 = a + \delta_v - ab$. Clearly, λ_1 and λ_2 are negative. By Routh–Hurwitz criteria [30], the eigenvalues λ_3 and λ_4 are negative if $a_1 > 0$ and $a_2 > 0$. Clearly, a_1 is positive, and for a_2 to be positive, we have $a_2 = a + \delta_v - ab > 0$, which implies $a < \frac{\delta_v}{b-1}$. Therefore, $E_1(1,\ 0,\ 0,\ 0)$ is stable if $a < \frac{\delta_v}{b-1}$ and is unstable if $> \frac{\delta_v}{b-1}$. □

Theorem 4. *The equilibrium point $E_2(x_2,\ y_2,\ v_2,\ 0)$ is locally asymptotically stable if $y_2 < \frac{\delta_z}{r_2}$ and $a < \frac{\delta_v(b+1)}{b-1} + 1$.*

Proof. The Jacobian matrix of the system (4) at $E_2(x_2,\ y_2,\ v_2,\ 0)$ is given by

$$J(E_2) = \begin{pmatrix} -r_1 - 2r_1x_2 - av_2 & 0 & -ax_2 & -k_1x_2 \\ av_2 & -1 & ax_2 & -k_2y_2 \\ -av_2 & b & -ax_2 - \delta_v & 0 \\ 0 & 0 & 0 & r_2y_2 - \delta_z \end{pmatrix}$$

The characteristic equation of $|J(E_2) - \lambda I| = 0$ is

$$p(\lambda) = (\lambda - (r_2y_2 - \delta_z))Q(\lambda). \tag{8}$$

where $Q(\lambda) = \lambda^3 + a_1\lambda^2 + a_2\lambda + a_3$ and

$$\begin{aligned} a_1 &= \tfrac{ab\delta_v + ab + r_1\delta_v - a}{a(b-1)}, \\ a_2 &= \tfrac{r_1\delta_v(b\delta_v + a + b + \delta_v - ab - 1)}{a(b-1)^2}, \\ a_3 &= \tfrac{r_1\delta_v(ab - a - \delta_v)}{a(b-1)}. \end{aligned} \tag{9}$$

After solving the characteristic Equation (8), we have $\lambda_1 = r_2y_2 - \delta_z$, and the other eigenvalues ($\lambda_{2,3,4}$) are the solutions of $Q(\lambda)$. It is clear that $a_1 > 0$ and $a_3 > 0$, since the equilibrium point E_2 exists if $b > 1$ and $a > \frac{\delta_v}{b-1}$. It is enough to show that $a_1 \cdot a_2 > a_3$ to prove that the eigenvalues $\lambda_{2,3,4}$ are negative by Routh–Hurwitz criteria.

Let $X = ab - a - \delta_v$, then

$$a_1 \cdot a_2 - a_3 = \frac{1}{a(b-1)^2}\left[\left(\frac{(ab + r_1)\delta_v}{a(b-1)} + 1\right)(b\delta_v + b - 1 - X) - (b-1)X\right],$$

$$a_1 \cdot a_2 - a_3 = \frac{1}{a(b-1)^2}\left[\left(\frac{(ab + r_1)\delta_v}{a(b-1)}\right)(b\delta_v + b - 1 - X) + b\delta_v + b - 1 - bX\right].$$

For $a_1 \cdot a_2 - a_3$ to be positive, we have $b\delta_v + b - 1 - X > 0$ and $b\delta_v + b - 1 - bX > 0$. We have $X < b\delta_v + b - 1$ since $b > 1$, which leads to $bX > X$. Therefore, we have the following condition. $X < b\delta_v + b - 1 \Rightarrow ab - a - \delta_v < b\delta_v + b - 1 \Rightarrow a(b-1) < \delta_v(b+1) + b - 1 \Rightarrow a < \frac{\delta_v(b+1)}{b-1} + 1$. Finally, we conclude that the eigenvalues of the Jacobian matrix at $E_2(x_2,\ y_2,\ v_2,\ 0)$ are negative if $\lambda_1 = r_2y_2 - \delta_z < 0$, which leads to $y_2 < \frac{\delta_z}{r_2}$ and $a < \frac{\delta_v(b+1)}{b-1} + 1$. □

Theorem 5. *The equilibrium point $E_3(x_3,\ y_3,\ v_3,\ z_3)$ is locally asymptotically stable provided $a_1 > 0,\ a_2 > 0,\ a_3 > 0,\ a_4 > 0$ and $a_1 \cdot a_2 \cdot a_3 > a_3^2 + a_1^2 \cdot a_4$.*

Proof. The Jacobian matrix of the system (4) at $E_3(x_3,\ y_3,\ v_3,\ z_3)$ gives

$$J(E_3) = \begin{pmatrix} -r_1x_3 & 0 & -ax_3 & -k_1x_3 \\ av_3 & -k_2z_3 - 1 & ax_3 & -k_2y_3 \\ -av_3 & b & -ax_3 - \delta_v & 0 \\ 0 & r_2z_3 & 0 & r_2y_3 - \delta_z \end{pmatrix}$$

The characteristic equation of $|J(E_3) - \lambda I| = 0$ is

$$p(\lambda) = \lambda^4 + a_1\lambda^3 + a_2\lambda^2 + a_3\lambda + a_4, \tag{10}$$

where

$$\begin{aligned}
a_1 = {} & ax_3 + k_2z_3 + r_1x_3 - r_2y_3 + \delta_v + \delta_z + 1 \\
a_2 = {} & -a^2x_3v_3 + ak_2x_3z_3 + ar_1x_3^2 - ar_2x_3y_3 + k_2r_1x_3z_3 - r_1r_2x_3y_3 - abx_3 + a\delta_zx_3 \\
& + k_2\delta_vz_3 + r_1\delta_vx_3 - r_2\delta_vy_3 + k_2\delta_zz_3 + r_1\delta_zx_3 + ax_3 + \delta_v\delta_z + r_1x_3 - r_2y_3 + \delta_v \\
& + \delta_z, \\
a_3 = {} & -a^2k_2x_3v_3z_3 + a^2r_2x_3y_3v_3 + ak_1r_2x_3v_3z_3 + ak_2r_1x_3^2z_3 - ar_1r_2x_3^2y_3 + a^2bx_3v_3 \\
& - a^2\delta_zx_3v_3 - abr_1x_3^2 + abr_2x_3y_3 + ak_2\delta_zx_3z_3 + ar_1\delta_zx_3^2 + k_2r_1\delta_vx_3z_3 \\
& - r_1r_2\delta_vx_3y_3 + r_1\delta_v\delta_zx_3z_3 - a^2x_3v_3 - ab\delta_zx_3 + ar_1x_3^2 - ar_2x_3y_3 + k_2\delta_v\delta_zz_3 \\
& + r_1\delta_v\delta_zx_3 - r_1r_2x_3y_3 + a\delta_zx_3 + r_1\delta_vx_3 - r_2\delta_vy_3 + r_1\delta_zx_3 + \delta_v\delta_z, \\
a_4 = {} & -a^2br_2x_3y_3v_3 - a^2k_2\delta_zx_3v_3z_3 + abr_1r_2x_3^2y_3 + ak_1r_2\delta_vx_3v_3z_3 + ak_2r_1\delta_zx_3^2z_3^2 \\
& + a^2b\delta_zx_3v_3 + a^2r_2x_3y_3v_3 - abr_1\delta_zx_3^2 - ar_1r_2x_3^2y_3 + k_2r_1\delta_v\delta_zx_3z_3 - a^2\delta_zx_3v_3 \\
& + ar_1\delta_zx_3^2 - r_1r_2\delta_vx_3y_3 + r_1\delta_v\delta_zx_3.
\end{aligned}$$

□

By the Routh–Hurwitz criterion, the asymptotic stability of $E_3(x_3,\ y_3,\ v_3,\ z_3)$ is guaranteed if the conditions stated in the theorem are satisfied.

Note that it is impossible to find conditions for E_3 to be asymptotically stable explicitly. We will show the stability of E_3 using the numerical results with various parameters.

2.4. Numerical Simulation

The nondimensionalized model (Equation (4)) is used to demonstrate the numerical results. The Runge–Kutta 2nd order method (modified Euler method) has been used to compute the numerical solutions with a time step $\Delta t = 0.05$ in MATLAB (The Mathworks, Natick, MA, US). We used smaller values of Δt to check the accuracy of the numerical method. For simulations, we used the values of the parameters that are taken from [20,27] and shown in Table 1. The populations (cancer cell, infected cancer cell, free virus and NK cell) are relative populations, and the time is also considered as the relative time, since all populations are divided by the carrying capacity of cancer cells and the time is multiplied by the death rate of infected cancer cells. After nondimensionalization, the values of the parameters in the system (Equation (4)) are

$$r_1 = 0.36,\ a = 0.1,\ k_1 = 0.36,\ k_2 = 0.48,\ r_2 = 0.6,\ \delta_v = 0.2,\ \delta_z = 0.36. \tag{11}$$

Table 1. The model parameters.

Parameter	Description	Value	Units	References
λ	Cancer growth rate	2×10^{-2}	1/h	[27]
α	Infection rate of the virus	$\frac{7}{10} \times 10^{-9}$	mm^3/h virus	[27]
β	Killing rate of cancer cells by NK cells	2.9×10^{-7}	mm^3/h NK cell	[20]
γ	Killing rate of infected cancer cells by NK cells	2.9×10^{-6}	mm^3/h NK cell	[20]
δ_1	Death rate of infected cancer cells	$\frac{1}{18}$	1/h	[27]
b	Burst rate of the virus	50	Viruses/cell	[27]
δ_2	Clearance rate of the virus	0.0118	1/h	[20]
λ_z	Stimulation (or activation) rate of the NK cells by infected cancer cells	5.6×10^{-7}	1/h infected cancer cell	[20]
δ_3	Clearance rate of NK cells	4.1×10^{-3}	1/h	[20]

3. Results

3.1. Existence and Stability of the Equilibrium Points

In numerical simulations, we used two initial conditions and changed some parameter values (b and r_2) to show the existence and stability of the equilibrium points. First, we changed parameters b and r_2 to 2 and 0.3, respectively; then, it satisfies the condition $a < \frac{\delta_v}{b-1}$ so that $E_1(1, 0, 0, 0)$ becomes asymptotically stable for two different sets of the initial conditions (Figure 1). This result indicates that the smaller bursting sizes in combination with the low stimulation rate of NK cells leads to the failure of therapy as cancer cells reach carrying capacity quickly. Second, when we increase the bursting size to b = 5 and maintain the same NK cell stimulation rate to $r_2 = 0.3$, the conditions for $E_2(x_2, y_2, v_2, 0)$ to be asymptotic stable are archived where $y_2 = 0.09 < \frac{\delta_z}{r_2} = 0.12$ and $a = 0.1 < \frac{\delta_v(b+1)}{b-1} + 1 = 1.3$. The solution $(x(t), y(t), v(t), z(t))$ converges to the equilibrium solution $E_2(0.5, 0.09, 1.8, 0)$ (Figure 2). This result indicates that the number of cancer cells is under control as the bursting size of viruses increases, although it cannot eliminate cancer cells. Finally, by increasing both the bursting size of viruses and the NK cell stimulation rate ($b = 5$ and $r_2 = 0.7$), the conditions for the existence and stability of $E_3(x_3, y_3, v_3, z_3)$ are satisfied. Thus, $E_3(0.5516, 0.0514, 1.0078, 0.1685)$ is asymptotically stable, as shown in Figure 3. Therefore, this result provides that our analytic and numerical results are in good agreement. We note that two equilibrium points $E_2(x_2, y_2, v_2, 0)$ and $E_3(x_3, y_3, v_3, z_3)$ do not exist in the positive invariant domain D if the equilibrium point $E_1(1, 0, 0, 0)$ is asymptotically stable. When $E_2(x_2, y_2, v_2, 0)$ becomes asymptotically stable, $E_1(1, 0, 0, 0)$ becomes unstable but $E_3(x_3, y_3, v_3, z_3)$ is still not in the domain D. Finally, when $E_3(x_3, y_3, v_3, z_3)$ is asymptotically stable, the other equilibrium points are in the positive invariant domain D, but they are all unstable.

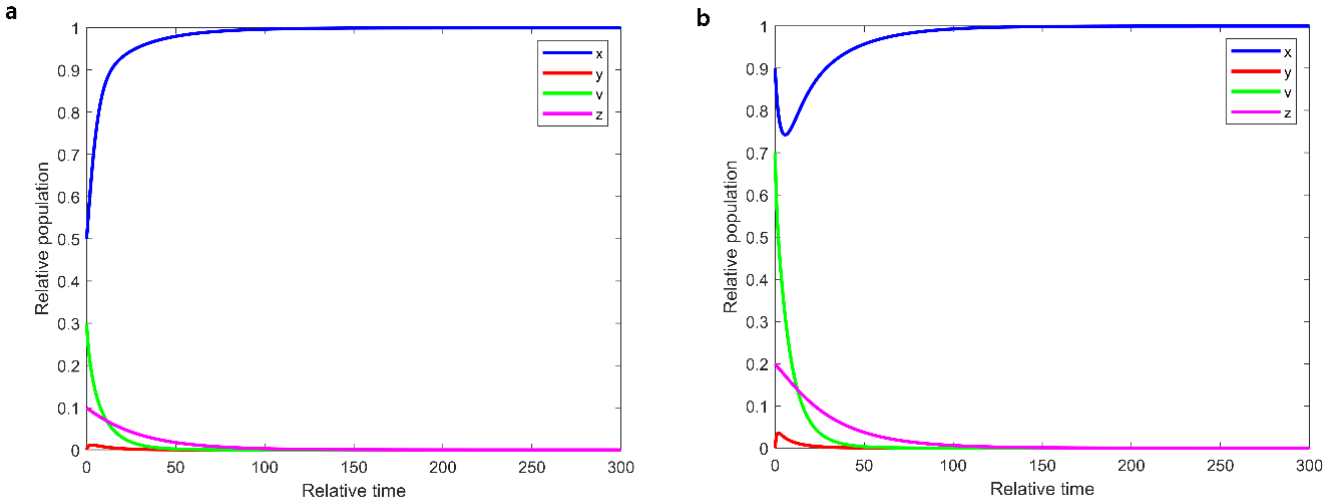


Figure 1. The relative population dynamics of cancer cells, infected cancer cells, virus and NK cells with respect to the relative time with two different initial conditions. (**a**) $x(0) = 0.5$, $y(0) = 0$, $v(0) = 0.3$, $z(0) = 0.1$ and (**b**) $x(0) = 0.9$, $y(0) = 0$, $v(0) = 0.7$, $z(0) = 0.2$. We used the parameters $r_1 = 0.36$, $a = 0.1, b = 2$, $k_1 = 0.36$ $k_2 = 0.48$, $r_2 = 0.3$, $\delta_v = 0.2$, $\delta_z = 0.036$.

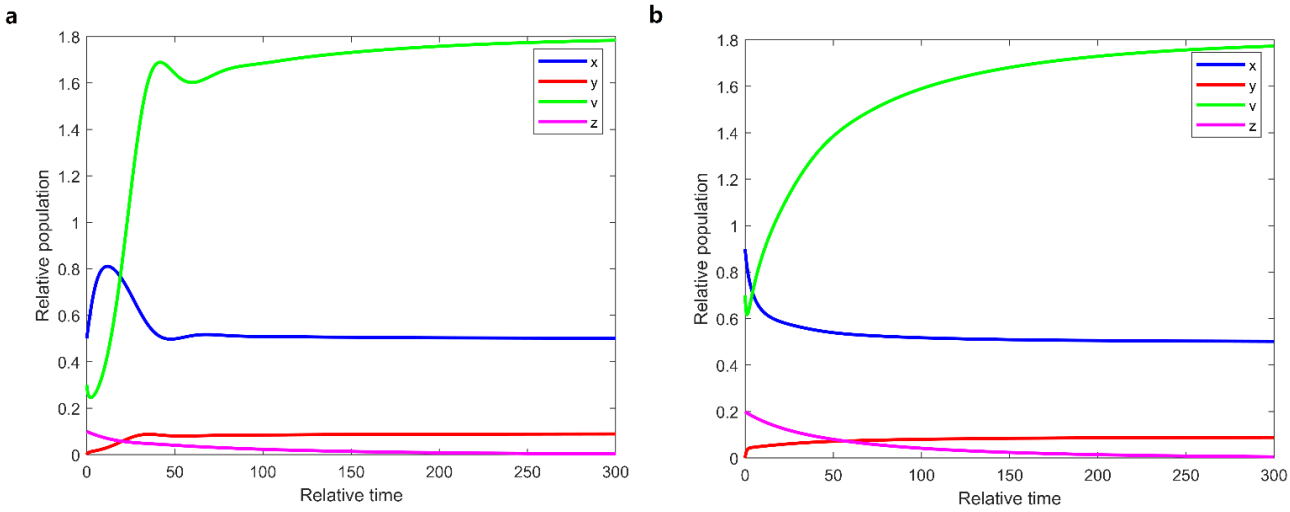


Figure 2. The relative population dynamics of cancer cells, infected cancer cells, virus and NK cells with respect to the relative time with two different initial conditions. (**a**) $x(0) = 0.5$, $y(0) = 0$, $v(0) = 0.3$, $z(0) = 0.1$ and (**b**) $x(0) = 0.9$, $y(0) = 0$, $v(0) = 0.7$, $z(0) = 0.2$. The population $(x(t), y(t), v(t), z(t))$ converges to the set (0.5, 0.09, 1.8, 0). We used the parameters $r_1 = 0.36$, $a = 0.1$, $b = 5$, $k_1 = 0.36$, $k_2 = 0.48$, $r_2 = 0.3$, $\delta_v = 0.2$, $\delta_z = 0.036$.

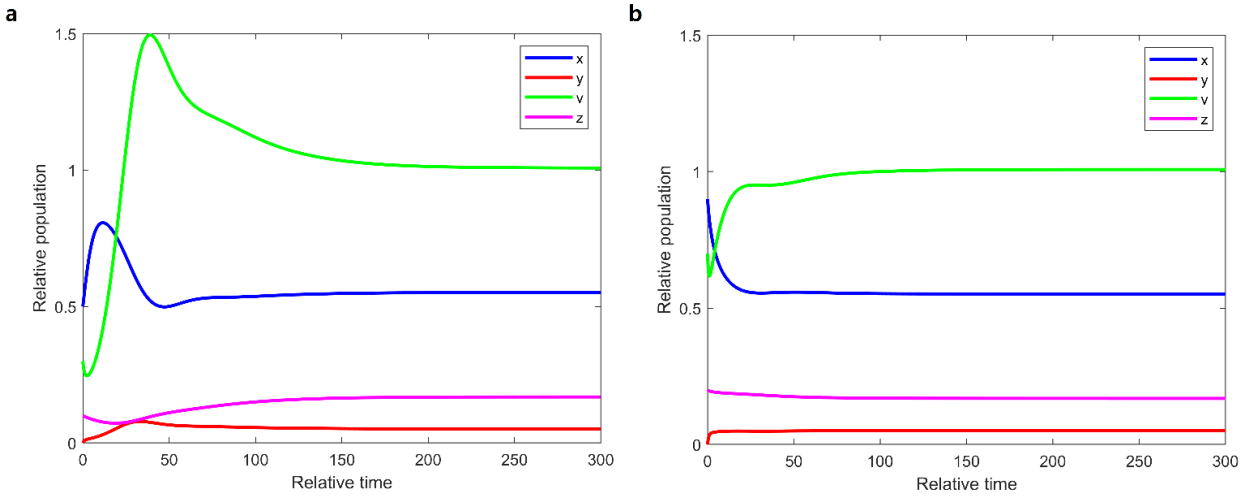


Figure 3. The relative population dynamics of cancer cells, infected cancer cells, virus and NK cells with respect to the relative time with two different initial conditions. (**a**) $x(0) = 0.5$, $y(0) = 0$, $v(0) = 0.3$, $z(0) = 0.1$ and (**b**) $x(0) = 0.9$, $y(0) = 0$, $v(0) = 0.7$, $z(0) = 0.2$. The population $(x(t), y(t), v(t), z(t))$ converges to the set (0.5516, 0.0514, 1.0078, 0.1685). We used the parameters $r_1 = 0.36$, $a = 0.1$, $b = 5$, $k_1 = 0.36$, $k_2 = 0.48$, $r_2 = 0.7$, $\delta_v = 0.2$, $\delta_z = 0.036$.

3.2. The Effect of NK Cell Activation on Population Dynamics

Figure 4 shows the effect of the stimulation rate of NK cells (r_2) on both the NK cells (Figure 4a) and the cancer cell populations (Figure 4b) with various values of b. We measured the equilibrium population of cancer cells and NK cells as r_2 varies from 0 to 2.0 with different values of $b = 0$, 5, 10 and 15. For $b = 0$, the population of stimulated NK cells tends to be 0 after the initial fluctuation by initial conditions. In other words, NK cells are not activated if there is no virus replication even if the stimulation rate of NK cells is high enough, suggesting that NK cells are only activated by infected cancer cells but not by viruses. When we set $b = 5$, the equilibrium population of NK cells gradually increases from $r_2 = 0.4$. For higher values of b, the activation of NK cells requires higher values of r_2 and the increasing rate (the slope of the curve) of the equilibrium population of NK cells

over r_2, which is higher than the rate at lower values of b (Figure 4a). Moreover, when NK cells activate, where the equilibrium population of NK cells is larger than 0, the equilibrium cancer cell population increased from the equilibrium population in the absence of NK cells (Figure 4b). Our results display that there are necessary conditions of parameter sets in b and r_2 for NK cells to exist and activate in the system, resulting in increasing the cancer cell population in the set of parameters.

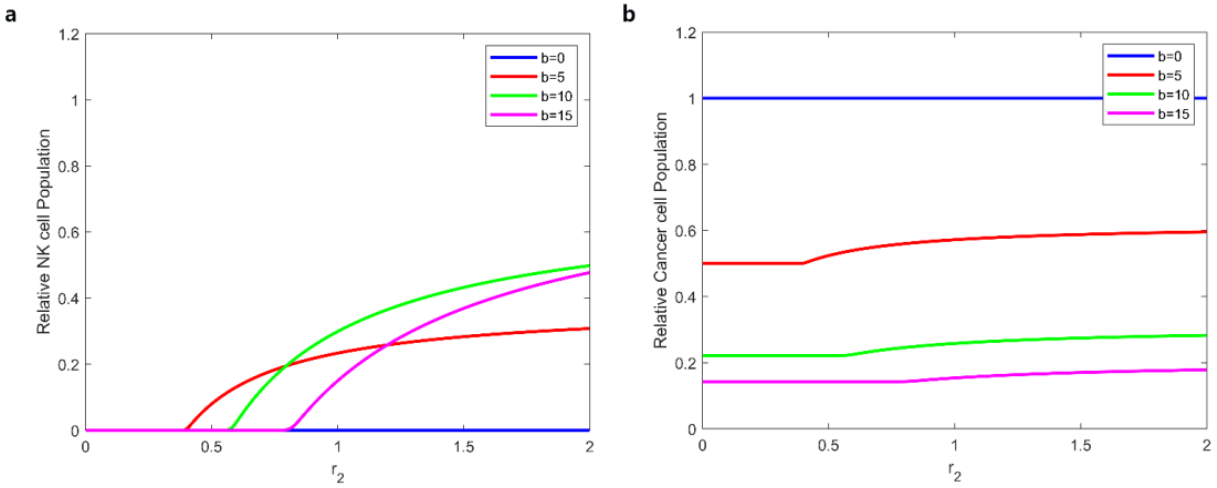


Figure 4. The equilibrium populations of the relative NK cells (**a**) and the relative cancer cells (**b**) over r_2 ranged from 0 to 2 with the bursting size of the virus b = 0, 5, 10 and 15. The NK cells are stimulated or activated within different ordered parameter sets (b, r_2). The equilibrium population of NK cells increases gradually at r_2 = 0.4, 0.58 and 0.8 when b = 5, 10 and 15, respectively. The result illustrates that there are necessary conditions in choosing parameters where NK cells activate and affect the efficacy of oncolytic virotherapy: Once the NK cells are activated, the cancer cell population increases, which leads to the reduction in efficacy of OV. We used the parameters $r_1 = 0.36$, $a = 0.1$, $k_1 = 0.36$, $k_2 = 0.48$, $\delta_v = 0.2$, $\delta_z = 0.36$.

Figure 5 shows the equilibrium populations of cancer cell (blue), infected cancer cell (red), free virus particles (green) and NK cells (purple) over r_2, which ranged from 0 to 3.0 at b = 5. The shape of equilibrium population curves changes at r_2 = 0.4, where stimulated NK cells start playing their role (activation) in the system. For example, the equilibrium population of virus and infected cancer cells decreases, but the equilibrium population of both cancer cells and NK cells increases as r_2 increased from 0.4. This result illustrates that higher values of r_2 recruit more NK cells, resulting in destroying the infected cancer cell before oncolysis, which leads to a decrease in the free virus particles. From a mathematical point of view, the critical value ($r_2^* = 0.4$) in r_2 is a bifurcation point at which the stability of the equilibrium point changed. The equilibrium point $E_2(x_2, y_2, v_2, 0)$ is asymptotically stable for $r_2 < r_2^*$. However, the equilibrium point $E_3(x_3, y_3, v_3, z_3)$ is asymptotically stable and point $E_2(x_2, y_2, v_2, 0)$ becomes unstable for $r_2 > r_2^*$, which indicates a transcritical bifurcation occurred at $r_2 = r_2^*$.

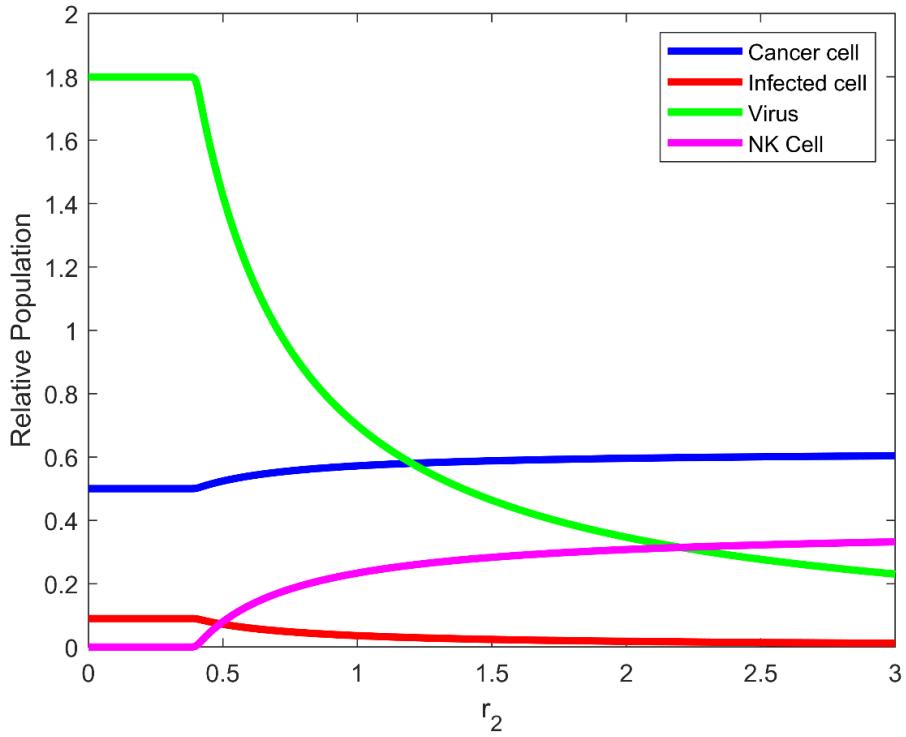


Figure 5. The change of dynamic structure of equilibrium populations at the critical value, $r_2 = r_2^* = 0.4$. The equilibrium populations of cancer cells (blue), infected cancer cells (red), virus (green) and NK cells (magenta) are changed at $r_2 = r_2^*$. The equilibrium populations of both cancer cells and NK cells gradually increase, but the other populations decay for $r_2 > r_2^*$, in other words, increasing r_2 reduces the infected cancer cell and virus population, but it increases the cancer cell and NK cell population. We used the parameters $r_1 = 0.36$, $a = 0.1$, $b = 5$, $k_1 = 0.36$, $k_2 = 0.48$, $\delta_v = 0.2$, $\delta_z = 0.36$.

3.3. Activation of NK Cells Reduces the Efficacy of Oncolytic Virotherapy, Requiring a Higher Bursting Rate of Virus to Generate Oscillations in the Cancer Cell Population

In this section, we investigated how two parameters (b and r_2) have an impact on the equilibrium population of cancer cells. For experiment simulations, we measured the equilibrium population of cancer cells over b from 0 to 30 with a step size of 0.01 with various values of $r_2 = 0,\ 0.5,\ 1.0$ and 1.5. We computed the equilibrium population of cancer cells as a function of b and plotted it as a curve in Figure 6a. The graph shows two changes in the shape of the equilibrium population of cancer cells: (1) from a horizontal line $x(t) = 1$ to monotonic decreasing curve and (2) from the decreasing curve to two curves where the population oscillates. Particularly, the equilibrium population of cancer cells is along the horizontal line, $x(t) = 1$, for $b \in [0,\ 3]$ and $r_2 \geq 0$. This result indicates that the therapy always fails for all $r_2 \geq 0$ if the bursting size of the virus is too low even with a higher stimulation rate value. For $b > 3$, the equilibrium cancer cell population gradually decreases as b increases until b approaches a critical value of b^* where the equilibrium cancer cell population oscillates between two values. The equilibrium population of NK cells over b is shown in Figure 6b. When $r_2 = 0.5$, NK cells are activated within a particular bursting size interval, $4 \leq b \leq 7$. For the higher values of r_2, the activation of NK cells starts at $b = 3.1$, and the interval of NK cell activation in b is becoming longer. Our numerical results show that for $3 < b < b^*$, the equilibrium cancer cell population is higher as r_2 increases, which suggests that the NK cells reduce the efficacy of OV. Moreover, the critical value b^* is becoming large when r_2 increases, which implies that the higher value of bursting size is required for the cancer cell population to show an oscillating pattern as r_2 increases.

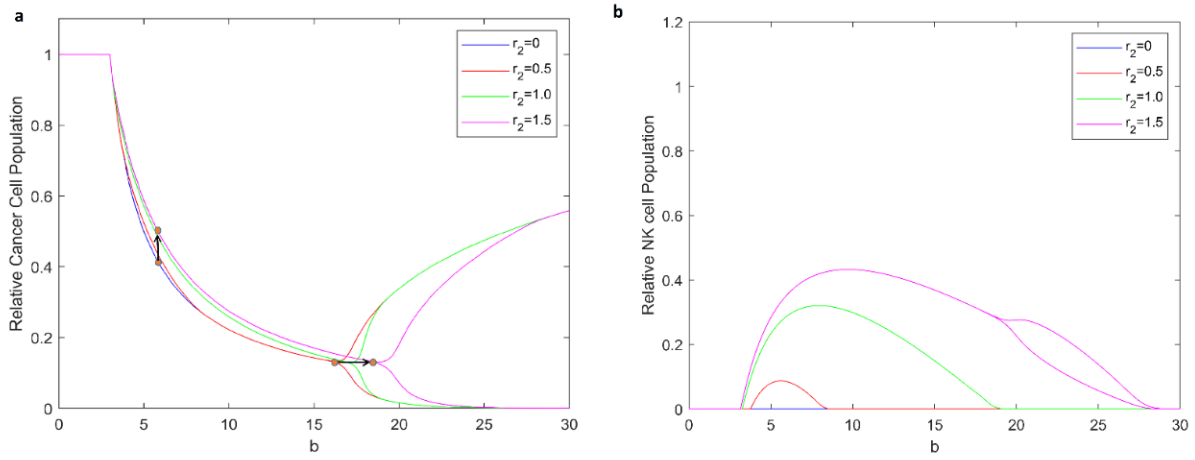


Figure 6. As r_2 increases, the equilibrium cancer cell increases and shows oscillation at a higher value of bursting rate. The vertical arrow shows the change of the equilibrium cancer cell population and the horizontal arrow shows the change of the virus bursting rate to show oscillatory pattern in the equilibrium cancer cell population from $r_2 = 0$ to $r_2 = 1.5$. The equilibrium cancer cell and NK cell over the bursting rate of virus b with different values of r_2 are shown in (**a**,**b**), respectively. We measured the relative equilibrium population of cancer cells with various values of r_2 = 0, 0.5, 1.0 and 1.5 when b varies from 0 to 30. Here, we used the parameters $r_1 = 0.36$, $a = 0.1$, $k_1 = 0.36$, $k_2 = 0.48$, $\delta_v = 0.2$, $\delta_z = 0.036$.

3.4. The Stability of Equilibrium Points Depends on the Existence of NK Cells

We have shown that the activation of NK cells in an OV system reduces the efficacy of the therapy. Here, we investigate the underlying mechanism of the role of NK cells in OV using the stability of equilibrium points. To show the effect of NK cells on OV in a dynamical system, we calculated the stability of the equilibrium points for each b with different values of r_2 and simulated the equilibrium population of cancer cells over b, which ranged from 0 to 30, with two scenarios: (a) no activation of NK cells by setting $r_2 = 0.3$ and (b) activation of NK cells by setting $r_2 = 0.7$, as shown in Figure 7. The stability of equilibrium points for various values of r_2 with respect to bursting size interval is given in Table 2. NK cells tend to 0 as the time increases at $r_2 = 0$. In this case, there are two critical values in b (called b_1 and b_2). A transcritical bifurcation occurs at $b = b_1$ where the stability changes from $E_1(1,\ 0,\ 0,\ 0)$ to $E_2(x_2,\ y_2,\ v_2,\ 0)$, and a Hopf bifurcation happens at $b = b_2$ where there is a limit cycle around $E_2(x_2,\ y_2,\ v_2,\ 0)$ (Figure 7a). However, the NK cells are shown in b $\in [3.41,\ 12.5]$ for $r_2 = 0.7$, and additional two critical values in b are created, at which the stability of equilibrium points change, appearing before and after the existence of NK cells (Figure 7b). More details are shown in Table 2. First, when $r_2 < 0.43$, the equilibrium cancer cell population for each b is governed by two equilibrium points (E_1 and E_2) and there are two critical values of b (b_1 and b_2), where $E_1(1,\ 0,\ 0,\ 0)$ is asymptotically stable for $b < b_1$ and $E_2(x_2,\ y_2,\ v_2,\ 0)$ is asymptotically stable for $b_1 < b < b_2$. There exists a limit cycle around $E_2(x_2,\ y_2,\ v_2,\ 0)$ where the populations exhibit oscillations for $b > b_2$ (Figure 7a). Second, when $0.43 \leq r_2 < 1.0$, there exist four critical values in b (called $b_1,\ b_2,\ b_3,\ b_4$,) where transcritical bifurcations happen at $b = b_1,\ b_2,\ b_3$ and a Hopf bifurcation happens at $b = b_4$. Particularly, $E_1(1,\ 0,\ 0,\ 0)$ is asymptotically stable for $b < b_1$, $E_2(x_2,\ y_2,\ v_2,\ 0)$ is asymptotically stable for $b_1 < b < b_2$, $E_3(x_3,\ y_3,\ v_3,\ z_3)$ is asymptotically stable for $b_2 < b < b_3$, $E_2(x_2,\ y_2,\ v_2,\ 0)$ is asymptotically stable for $b_3 < b < b_4$, and there exists a limit cycle around $E_2(x_2,\ y_2,\ v_2,\ 0)$ where three populations ($x(t)$, $y(t)$ and $v(t)$) oscillate, but NK cells tend to zero population. Note that when $r_2 = 1.0$, there exist three critical values in b where $E_1(1,\ 0,\ 0,\ 0)$ is asymptotically stable in b $\leq b_1 = 3$, $E_2(x_2,\ y_2,\ v_2,\ 0)$ is asymptotically stable in $b_1 < b \leq b_2 = 3.2$, $E_3(x_3,\ y_3,\ v_3,\ z_3)$ is asymptotically stable in $b_2 < b \leq b_3 = 17.7$ and there is a limit cycle around $E_3(x_3,\ y_3,\ v_3,\ z_3)$ where all populations oscillate for $b > b_3$.

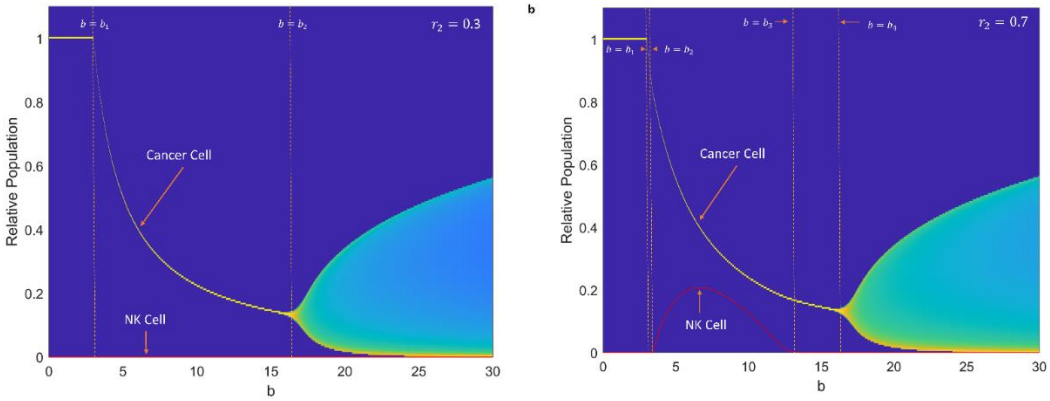


Figure 7. Two-dimensional (2D) bifurcation diagram of the equilibrium cancer cell population with respect to the bifurcation parameter b with or without the existence of NK cells. The bifurcation values in b can be created or destroyed depending on the activation of NK cells. We simulated and calculated the equilibrium cancer cell population over b, which ranged from 0 to 30, with two scenarios: (**a**) no activation of NK cells when $r_2 = 0.3$ and (**b**) activation of NK cells when $r_2 = 0.7$. Here, we used the parameters $r_1 = 0.36$, $a = 0.1$, $k_1 = 0.36$, $k_2 = 0.48$, $\delta_v = 0.2$, $\delta_z = 0.036$.

Table 2. Stability of Equilibrium Points: Transcritical and Hopf Bifurcations.

r_2	Interval of b	Stability of E_1 (0, 0, 0, 0)	Stability of $E_2(x_2, y_2, v_2, 0)$	Stability of $E_3(x_3, y_3, v_3, z_3)$
0.43	$0 < b \leq 3$	Stable	Unstable	Unstable
	$3 < b \leq 4.2$	Unstable	Stable	Unstable
	$4.2 < b \leq 6.4$	Unstable	Unstable	Stable
	$6.4 < b \leq 17.1$	Unstable	Stable	Unstable
	$b > 17.1$	Unstable	Limit cycle	Unstable
0.5	$0 < b \leq 3$	Stable	Unstable	Unstable
	$3 < b \leq 3.7$	Unstable	Stable	Unstable
	$3.7 < b \leq 8.2$	Unstable	Unstable	Stable
	$8.2 < b \leq 17.1$	Unstable	Stable	Unstable
	$b > 17.1$	Unstable	Limit cycle	Unstable
0.6	$0 < b \leq 3$	Stable	Unstable	Unstable
	$3 < b \leq 3.6$	Unstable	Stable	Unstable
	$3.6 < b \leq 10.5$	Unstable	Unstable	Stable
	$10.5 < b \leq 17.1$	Unstable	Stable	Unstable
	$b > 17.1$	Unstable	Limit cycle	Unstable
0.7	$0 < b \leq 3$	Stable	Unstable	Unstable
	$3 < b \leq 3.4$	Unstable	Stable	Unstable
	$3.3 < b \leq 12.5$	Unstable	Unstable	Stable
	$12.5 < b \leq 17.1$	Unstable	Stable	Unstable
	$b > 17.1$	Unstable	Limit cycle	Unstable
0.8	$0 < b \leq 3$	Stable	Unstable	Unstable
	$3 < b \leq 3.3$	Unstable	Stable	Unstable
	$3.3 < b \leq 14.6$	Unstable	Unstable	Stable
	$14.6 < b \leq 17.1$	Unstable	Stable	Unstable
	$b > 17.1$	Unstable	Limit cycle	Unstable

Interestingly, the length of the second interval $b_1 < b < b_2$ approaches to zero as r_2 increases. In other words, when r_2 is high enough where NK cells activate and play their natural roles in killing the targeted cancer cell and infected cancer cell, the free NK cell equilibrium point $E_2(x_2,\ y_2,\ v_2,\ 0)$ loses its stability, and the population dynamics of the system is governed by $E_3(x_3,\ y_3,\ v_3,\ z_3)$ where all populations coexist, and the equilibrium cancer cell population is higher than the population without NK cells, which supports that NK cells reduce the efficacy of OV.

3.5. Two Parameters (b and r_2) Bifurcation Diagram

The qualitative changes in the stability of equilibrium points or in which the equilibrium points are created or destroyed depending on parameters are called bifurcation in dynamical systems. The capability of virus to produce new virus particles and the viral infection play important roles in OV, since the bursting size and the strength of infectivity of virus change the stability of equilibrium points, creating or destroying equilibrium points. Our numerical results show that our model undergoes complex bifurcation in a dynamical system at multiple critical values of b, depending on the existence of NK cells in the system; more bifurcation values of b are created in the presence of NK cells, which indicates r_2 can be considered as a bifurcation value. In this section, we investigated the stability of equilibrium points and computed two-parameter bifurcation diagrams illustrating how our nonlinear model behaves when two parameters of our model vary simultaneously. In the simulations, we computed the stability of equilibrium points by varying b and r_2 with a fixed value of a. Then, we plotted the stability region of equilibrium points and the regions of periodic solutions in two-dimensional parameter space.

For simulations, we calculated the eigenvalue of a Jacobian matrix at each equilibrium point for each parameter and plotted in the rectangular coordinate (r_2b-plane). We set the parameters given in (10) and varied b from 0 to 20 with a step size $\Delta b = 0.1$ (y-axis) and r_2 from 0 to 3 with a step size $\Delta r_2 = 0.01$ (x-axis) in Figure 8. Our result shows four different colored regions which represent the following: (1) the dark blue region is the set of parameters (r_2, b) at which the relative cancer cell population converges to the maximal carrying capacity and other cell populations converge to zero over time ($E_1(1,\ 0,\ 0,\ 0)$ is asymptotically stable in the dark blue area), (2) the light blue one is the region where the relative populations of cancer cells, infected cancer cells and virus exhibit damped oscillations over time and converge to the free NK cell equilibrium point $E_2(x_2,\ y_2,\ v_2,\ 0)$, (3) the green one is the region where all relative populations show damped oscillations over time and converge to the equilibrium point $E_3(x_3,\ y_3,\ v_3,\ z_3)$, (4) three populations oscillate (no NK cells exist) over time in the orange area and (5) four populations oscillate (including NK cells) over time in the yellow area. As shown in the two-dimensional bifurcation diagram, therefore, it is very clear to see where bifurcations happen and what type of bifurcations occurs. For example, transcritical bifurcations occur at the border between the light blue and green-colored shaded regions, and other transcritical bifurcations occur at the borderline between the dark blue and light blue-colored shaded regions. Hopf bifurcations arise at the border between the light blue and orange-colored regions and at the border between the green and yellow-colored regions. Particularly, for $0 \leq r_2 < 0.91$, the OV partially succeeds, and the cancer cell population decreases up to minimum population $x(t) = 0.12$ from the initial condition $x(0) = 0.5$ at $b = 17.1$ (borderline between the light blue and orange area). For $r_2 > 0.91$ and b = 17.1, the population dynamics is governed by $E_3(x_3,\ y_3,\ v_3,\ z_3)$ and the cancer cell population slightly increases (green region) or all populations oscillate (yellow region) due to interference by NK cells in OV.

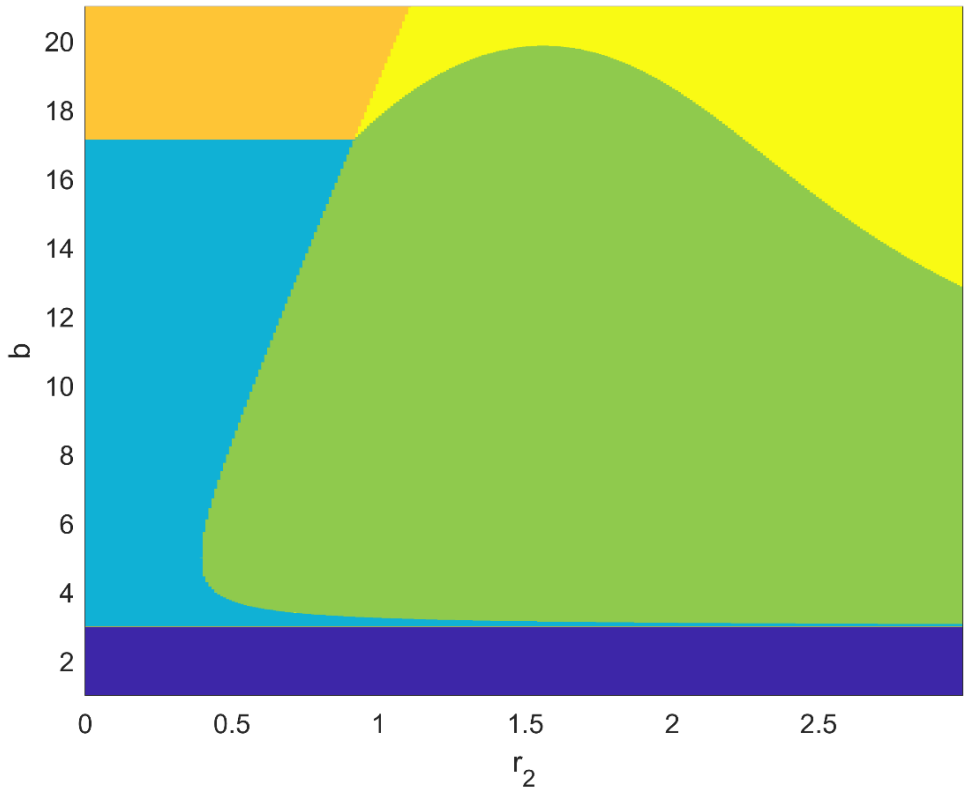


Figure 8. Stability region of equilibrium points with respect to two parameters (b and r_2). E_1 is asymptotically stable in the dark blue region, E_2 is asymptotically stable in the light blue region, E_3 is asymptotically stable in the green region, three populations (x, y, v) oscillate over time in the orange region, and all populations oscillate over time in the yellow region. The relative cancer cell population shows minimum population at the border between the light blue and orange-colored regions. The result illustrates a whole picture for the number of bifurcation points when either r_2 or b varies.

4. Discussion

In this study, we established a simple mathematical model to simulate the interaction among cancer cells, oncolytic viruses, infected cancer cells, and NK cells stimulated by either infected cancer cells or oncolytic viruses. We provided the existence and boundness of solutions. We used the local stability analysis to examine the dynamics of population among cancer cells, infected cancer cells, oncolytic virus and NK cells. As a result, the existence and stability of equilibrium is dependent on the parameters, and the bifurcation threshold values of bursting rate can be created or destroyed depending on the activation of NK cells, which also indicates that the activation rate of NK cells acts as a bifurcation parameter.

In our experiments, we identified threshold values of the activation of NK cells where NK cell activation is sufficient to switch from an NK cell-free equilibrium (E_2) to the presence of NK cells (E_3). The NK cell activation rate, which is larger than the threshold ($r_2 > r_2^*$), also resulted in increasing cancer cell populations due to the clearance of OV-infected cancer cells leading to a loss of OV efficacy. Therefore, in relation to increasing NK cell stimulation values, a higher value of bursting rates of the virus is required to achieve the same relative cancer cell population, while small bursting rates result in therapy failure irrespective of NK cell stimulation. In addition, higher bursting rates are required at increasing stimulation rates to reach an oscillation of the cancer cell population. The NK cell stimulation value with respect to reaching an NK cell equilibrium population larger than 0 was then shown to define the presence or absence of additional bifurcation values for the bursting rate. Two-dimensional bifurcation in the stability of equilibrium points was performed on the following parameters: the bursting rate (b) and the stimulation rate

(r_2). Our two-dimensional bifurcation diagram provides a promising result in determining optimal parameters for the successful therapy. Finally, the model may be extended to an oncolytic virotherapy with macrophage and NK cells, since M1 macrophages recruit and activate NK cells [31,32]. Future investigation may focus on the development of a mathematical model to analyze the effects of the combination of NK cells and macrophages on oncolytic virotherapy.

Recently, Senekal et al. showed the effect of NK cell recruitment on oncolytic virotherapy using a mathematical model. Their results demonstrated that the OV therapy efficacy depends on the viral cytopathicity and the recruitment of NK cells that regulate tumor growth [26]. Our study focused on not only the effect of NK cell activation on the dynamics of populations but also the relationship between virus bursting rate and NK cell activation and how those parameters change the dynamic structure by finding the stability of equilibrium points and bifurcation values in both parameters. In our initial analysis, the infection rate and half-life of viruses also showed similar effects as the bursting size does on controlling cancer cell population during OV therapy. The activation or non-activation of NK cells can create or destroy equilibrium points, which leads to different results in the therapy.

For oncolytic virotherapies, there have been two contradictory observations both in clinical trials and biological experiments. In one study, triggering an immune response by oncolytic viruses promoted the elimination of cancer cells, suggesting that the patient's immune system is crucial for the success of oncolytic virotherapy. In another study, however, triggering patient's immune response including NK cells diminished the efficacy of oncolytic virotherapy. It has been suggested that activated NK cells can destroy infected cancer cells prematurely and interfere with the reproduction of viruses.

In subsequent analyses, we also discovered that the activation of NK cells has a negative effect on OV therapy by reducing the viral population greater than cancer cell population. To understand the dynamic interaction among NK cells, infected cancer cells, and viruses, we adjusted the activation rate of NK cells by applying various bursting sizes and infection rates. In this process, we have observed that equilibrium points can be created or destroyed by the activation rate of NK cells and the provided parameter bifurcation regions using the two-dimensional bifurcation diagram.

Although there are several other immune cells affecting OVs, our results suggest that large bursting sizes or high infection rates of OVs can prematurely activate NK cells that lead to the elimination of infected cancer cells, resulting in a reduced production of OVs after the initial administration. To avoid this premature elimination of infected cancer cells by NK cells, cotreatment with NK inhibitors can be considered. Another possible approach would be the mesenchymal progenitor cells (MPC)-vehicle method [33]. In this method, increased oncoviral efficacy was achieved with MPC vectors containing replication-competent adenovirus, not provoking too much immune responses.

Author Contributions: Conceptualization, D.K.; methodology, D.K.; software, D.K.; validation, D.K. and C.K.S.; formal analysis, D.K. and D.-H.S.; investigation, D.K.; data curation, D.K and C.K.S.; writing—original draft preparation, D.K and C.K.S.; writing—review and editing, D.K., D.-H.S. and C.K.S.; supervision, D.K.; project administration, D.K.; funding acquisition, D.K. All authors have read and agreed to the published version of the manuscript.

Funding: This research received no external funding.

Data Availability Statement: Not applicable.

Acknowledgments: The author would like to thank Haeyoung Kim for useful discussion and great feedback.

Conflicts of Interest: The authors declare no conflict of interest.

References

1. Parato, K.A.; Breitbach, C.J.; Le Boeuf, F.; Wang, J.; Storbeck, C.; Ilkow, C.; Diallo, J.S.; Falls, T.; Burns, J.; Garcia, V.; et al. The oncolytic poxvirus JX-594 selectively replicates in and destroys cancer cells driven by genetic pathways commonly activated in cancers. *Mol. Ther.* **2012**, *20*, 749–758. [CrossRef] [PubMed]
2. Huang, Z.; Liu, M.; Huang, Y. Oncolytic therapy and gene therapy for cancer: Recent advances in antitumor effects of Newcastle disease virus. *Discov. Med.* **2020**, *30*, 39–48. [PubMed]
3. Kazemi Shariat Panahi, H.; Dehhaghi, M.; Lam, S.S.; Peng, W.; Aghbashlo, M.; Tabatabaei, M.; Guillemin, G.J. Oncolytic viruses as a promising therapeutic strategy against the detrimental health impacts of air pollution: The case of glioblastoma multiforme. *Semin. Cancer Biol.* 2021, *in press*. [CrossRef] [PubMed]
4. Mondal, M.; Guo, J.; He, P.; Zhou, D. Recent advances of oncolytic virus in cancer therapy. *Hum. Vaccines Immunother.* **2020**, *16*, 2389–2402. [CrossRef]
5. Thorne, S.H.; Hwang, T.H.; O'Gorman, W.E.; Bartlett, D.L.; Sei, S.; Kanji, F.; Brown, C.; Werier, J.; Cho, J.H.; Lee, D.E.; et al. Rational strain selection and engineering creates a broad-spectrum, systemically effective oncolytic poxvirus, JX-963. *J. Clin. Investig.* **2007**, *117*, 3350–3358. [CrossRef]
6. Eissa, I.R.; Bustos-Villalobos, I.; Ichinose, T.; Matsumura, S.; Naoe, Y.; Miyajima, N.; Morimoto, D.; Mukoyama, N.; Zhiwen, W.; Tanaka, M.; et al. The Current Status and Future Prospects of Oncolytic Viruses in Clinical Trials against Melanoma, Glioma, Pancreatic, and Breast Cancers. *Cancers* **2018**, *10*, 356. [CrossRef]
7. Ferrucci, P.F.; Pala, L.; Conforti, F.; Cocorocchio, E. Talimogene Laherparepvec (T-VEC): An Intralesional Cancer Immunotherapy for Advanced Melanoma. *Cancers* **2021**, *13*, 1383. [CrossRef]
8. Gesundheit, B.; Ben-David, E.; Posen, Y.; Ellis, R.; Wollmann, G.; Schneider, E.M.; Aigner, K.; Brauns, L.; Nesselhut, T.; Ackva, I.; et al. Effective Treatment of Glioblastoma Multiforme With Oncolytic Virotherapy: A Case-Series. *Front. Oncol.* **2020**, *10*, 702. [CrossRef]
9. Desjardins, A.; Gromeier, M.; Herndon, J.E., 2nd; Beaubier, N.; Bolognesi, D.P.; Friedman, A.H.; Friedman, H.S.; McSherry, F.; Muscat, A.M.; Nair, S.; et al. Recurrent Glioblastoma Treated with Recombinant Poliovirus. *N. Engl. J. Med.* **2018**, *379*, 150–161. [CrossRef]
10. Filley, A.C.; Dey, M. Immune System, Friend or Foe of Oncolytic Virotherapy? *Front. Oncol.* **2017**, *7*, 106. [CrossRef]
11. Al-Tuwairqi, S.M.; Al-Johani, N.O.; Simbawa, E.A. Modeling dynamics of cancer virotherapy with immune response. *Adv. Differ. Equ.* **2020**, *2020*, 438. [CrossRef]
12. Shi, T.; Song, X.; Wang, Y.; Liu, F.; Wei, J. Combining Oncolytic Viruses With Cancer Immunotherapy: Establishing a New Generation of Cancer Treatment. *Front. Immunol.* **2020**, *11*, 683. [CrossRef]
13. Leung, E.Y.L.; Ennis, D.P.; Kennedy, P.R.; Hansell, C.; Dowson, S.; Farquharson, M.; Spiliopoulou, P.; Nautiyal, J.; McNamara, S.; Carlin, L.M.; et al. NK Cells Augment Oncolytic Adenovirus Cytotoxicity in Ovarian Cancer. *Mol. Ther. Oncolytics* **2020**, *16*, 289–301. [CrossRef]
14. Li, X.; Wang, P.; Li, H.; Du, X.; Liu, M.; Huang, Q.; Wang, Y.; Wang, S. The Efficacy of Oncolytic Adenovirus Is Mediated by T-cell Responses against Virus and Tumor in Syrian Hamster Model. *Clin. Cancer Res.* **2017**, *23*, 239–249. [CrossRef]
15. Lemos de Matos, A.; Franco, L.S.; McFadden, G. Oncolytic Viruses and the Immune System: The Dynamic Duo. *Mol. Ther. Methods Clin. Dev.* **2020**, *17*, 349–358. [CrossRef]
16. Leung, E.Y.L.; McNeish, I.A. Strategies to Optimise Oncolytic Viral Therapies: The Role of Natural Killer Cells. *Viruses* **2021**, *13*, 1450. [CrossRef]
17. Alvarez-Breckenridge, C.A.; Yu, J.; Price, R.; Wojton, J.; Pradarelli, J.; Mao, H.; Wei, M.; Wang, Y.; He, S.; Hardcastle, J.; et al. NK cells impede glioblastoma virotherapy through NKp30 and NKp46 natural cytotoxicity receptors. *Nat. Med.* **2012**, *18*, 1827–1834. [CrossRef]
18. Han, J.; Alvarez-Breckenridge, C.A.; Wang, Q.E.; Yu, J. TGF-beta signaling and its targeting for glioma treatment. *Am. J. Cancer Res.* **2015**, *5*, 945–955.
19. Altomonte, J.; Wu, L.; Meseck, M.; Chen, L.; Ebert, O.; Garcia-Sastre, A.; Fallon, J.; Mandeli, J.; Woo, S.L. Enhanced oncolytic potency of vesicular stomatitis virus through vector-mediated inhibition of NK and NKT cells. *Cancer Gene Ther.* **2009**, *16*, 266–278. [CrossRef]
20. Kim, Y.; Yoo, J.Y.; Lee, T.J.; Liu, J.; Yu, J.; Caligiuri, M.A.; Kaur, B.; Friedman, A. Complex role of NK cells in regulation of oncolytic virus-bortezomib therapy. *Proc. Natl. Acad. Sci. USA* **2018**, *115*, 4927–4932. [CrossRef]
21. Mahasa, K.J.; de Pillis, L.; Ouifki, R.; Eladdadi, A.; Maini, P.; Yoon, A.R.; Yun, C.O. Mesenchymal stem cells used as carrier cells of oncolytic adenovirus results in enhanced oncolytic virotherapy. *Sci. Rep.* **2020**, *10*, 425. [CrossRef]
22. Macnamara, C.; Eftimie, R. Memory versus effector immune responses in oncolytic virotherapies. *J. Theor. Biol.* **2015**, *377*, 1–9. [CrossRef]
23. Phan, T.A.; Tian, J.P. The Role of the Innate Immune System in Oncolytic Virotherapy. *Comput. Math. Methods Med.* **2017**, *2017*, 6587258. [CrossRef]
24. Ikawati, D.S.E.; Kusumawinahyu, W.M.; Trisilowati. A Dynamical Analysis on a Tumour Virotherapy Model with Standard Incident Rate. *J. Trop. Life Sci.* **2016**, *7*, 16–22. [CrossRef]
25. Wodarz, D. Gene therapy for killing p53-negative cancer cells: Use of replicating versus nonreplicating agents. *Hum. Gene Ther.* **2003**, *14*, 153–159. [CrossRef]

26. Senekal, N.S.; Mahasa, K.J.; Eladdadi, A.; de Pillis, L.; Ouifki, R. Natural Killer Cells Recruitment in Oncolytic Virotherapy: A Mathematical Model. *Bull. Math. Biol.* **2021**, *83*, 75. [CrossRef]
27. Friedman, A.; Tian, J.P.; Fulci, G.; Chiocca, E.A.; Wang, J. Glioma virotherapy: Effects of innate immune suppression and increased viral replication capacity. *Cancer Res.* **2006**, *66*, 2314–2319. [CrossRef]
28. Kambara, H.; Okano, H.; Chiocca, E.A.; Saeki, Y. An oncolytic HSV-1 mutant expressing ICP34.5 under control of a nestin promoter increases survival of animals even when symptomatic from a brain tumor. *Cancer Res.* **2005**, *65*, 2832–2839. [CrossRef]
29. Tian, J.P. The replicability of oncolytic virus: Defining conditions in tumor virotherapy. *Math. Biosci. Eng.* **2011**, *8*, 841–860. [CrossRef]
30. Fuchs, B.A.; Levin, V.I. *Functions of a Complex Variable and Some of Their Applications*; Pergamon Press: London, UK, 1961; Volume II.
31. Hofman, L.; Lawler, S.E.; Lamfers, M.L.M. The Multifaceted Role of Macrophages in Oncolytic Virotherapy. *Viruses* **2021**, *13*, 1570. [CrossRef]
32. Mosser, D.M.; Edwards, J.P. Exploring the full spectrum of macrophage activation. *Nat. Rev. Immunol.* **2008**, *8*, 958–969. [CrossRef] [PubMed]
33. Komarova, S.; Kawakami, Y.; Stoff-Khalili, M.A.; Curiel, D.T.; Pereboeva, L. Mesenchymal progenitor cells as cellular vehicles for delivery of oncolytic adenoviruses. *Mol. Cancer Ther.* **2006**, *5*, 755–766. [CrossRef] [PubMed]